

# Aero-elastic response of transmission line system subjected to downburst wind: Validation of numerical model using experimental data

Amal Elawady<sup>1</sup>, Haitham Aboshosha<sup>2</sup> and Ashraf El Damatty<sup>\*3,4,5</sup>

<sup>1</sup>Department of Civil and Environmental Engineering, Florida International University, Miami, United States

<sup>2</sup>Department of Civil Engineering, Ryerson University, Toronto, Ontario, Canada

<sup>3</sup>Department of Civil and Environmental Engineering, Western University, London, Ontario, Canada

<sup>4</sup>The Wind Engineering, Energy and Environment (WindEEE) Research Institute, Western University, London, Ontario, Canada

<sup>5</sup>Department of Structural Engineering, Faculty of Engineering, Cairo University, Egypt

(Received March 2, 2018, Revised June 6, 2018, Accepted June 27, 2018)

**Abstract.** At the University of Western Ontario (UWO), numerical tools represented in semi-closed form solution for the conductors and finite element modeling of the lattice tower were developed and utilized significantly to assess the behavior of transmission lines under downburst wind fields. Although these tools were validated against other finite element analyses, it is essential to validate the findings of those tools using experimental data. This paper reports the first aeroelastic test for a multi-span transmission line under simulated downburst. The test has been conducted at the three-dimensional wind testing facility, the WindEEE dome, located at the UWO. The experiment considers various downburst locations with respect to the transmission line system. Responses obtained from the experiment are analyzed in the current study to identify the critical downburst locations causing maximum internal forces in the structure (i.e., potential failure modes), which are compared with the failure modes obtained from the numerical tools. In addition, a quantitative comparison between the measured critical responses obtained from the experiment with critical responses obtained from the numerical tools is also conducted. The study shows a very good agreement between the critical configurations of the downburst obtained from the experiment compared to those predicted previously by different numerical studies. In addition, the structural responses obtained from the experiment and those obtained from the numerical tools are in a good agreement where a maximum difference of 16% is found for the mean responses and 25% for the peak responses.

**Keywords:** aero-elastic modeling; downburst; transmission line; cable; wind load; high-intensity wind; WindEEE

## 1. Introduction

Downbursts are usually associated with thunderstorms and are defined as localized cold masses of air that impinge towards the ground and then convect horizontally causing high wind speeds (Fujita 1985). Those high wind speeds can lead to severe damage to various structures including transmission line structures which span over long distances to transport electricity from the source of production to the distributing network. The extension of transmission line systems for over many kilometers increases their vulnerability to be hit by downbursts. Many failure incidents of transmission lines/towers due to thunderstorms were reported in literature. Most recently in 2016, more than 20 transmission towers failed during a series of downburst events in South Australia (Australian Wind Alliance, 2016). In 2005, ten towers failed in JiangSu, China, during a severe thunderstorm as reported by Zhang (2006). Kanak *et al.* (2007) reported the failure of 18 power towers during a severe thunderstorm in Slovakia that occurred in 2003. Knowing that the failed lines were designed for a wind speed of 44 m/s, the study suggested that the failure of the power lines was due to downburst

events of a velocity higher than 44 m/s. In 1996, a series of transmission tower failures in Manitoba, Canada, under severe thunderstorms was reported by McCarthy and Melsness (1996). Similar incident occurred in Ontario, Canada where two 500 kV guyed towers failed during a severe thunderstorm (Hydro One 2006). The failure was found to be localized in these two towers only and none of the towers of the three other lines at the vicinity of the failed line were affected. Metrological analysis indicated that a high intensity microburst (i.e., small size downburst) associated with very high wind speeds of ~ 50 m/s took place in the zone of the failed towers (Hydro One 2006). Fig. 1 shows one of the failed towers. The lack of information regarding proper procedure for designing transmission line structures to resist downbursts in addition to the reoccurring failures of the transmission lines during thunderstorms motivated number of researchers to characterize the downburst wind field and to investigate the behavior of transmission line systems under downbursts.

Due to the spatial and temporal localization of downbursts, a limited number of downburst field measurements were reported in the literature such as Northern Illinois Meteorological Research (NIMROD) and the Joint Airport Weather Studies (JAWS) reported by Fujita (1990), the downburst that occurred near Lubbock, Texas in 2002 and reported by Holmes *et al.* (2008), and the Wind and Ports project reported by Solari *et al.* (2015). On the

\*Corresponding author, Professor  
E-mail: [damatty@uwo.ca](mailto:damatty@uwo.ca)

other hand, various small-scale experimental studies (such as by Donaldson and Snedeker 1971, Didden and Ho 1985, and Chay and Letchford 2002), and analytical studies (such as Oseguera and Bowles 1988, Chay *et al.* 2006, and Abd-Elaal *et al.* 2013) were conducted. Numerical simulations are another tools where various features of the downburst wind field can be modelled including the temporal and spatial variations and the roughness effect. Three numerical simulation approaches are found in the literature as follows: a) the Impinging Jet Simulations (such as by Chay *et al.* 2006, Kim and Hangan 2007, Sengupta and Sarkar 2008, Gant 2009, and Aboshosha *et al.* 2015); b) the Cooling Source simulations (such as by Mason *et al.*, 2009 and 2010, and Vermeire *et al.* 2011); and c) the Ring Vortex Simulations (such as by Ivan 1986 and Savory *et al.* 2001).

Despite the severity of downburst effects on transmission line structures, no sufficient information is available in the design guidelines to account for downbursts. Few number of studies investigated the effect of downburst winds on transmission line structures. Savory *et al.* (2001) conducted a failure analysis on a single transmission tower subjected to both tornado and downburst loads. The study reported that the considered tower was more vulnerable to tornado loading compared to downburst loading. However, this study did not consider the conductor forces, which are expected to be more significant in the case of downbursts because of their large size compared to tornadoes. Most of the structural studies, such as Wang *et al.* (2013), Yang and Zhang, (2016), and Mara *et al.* (2016), utilized the vertical wind profile of the peak radial velocity,  $V_{RD}$ , of the downburst while ignoring the spatial effect of downbursts. Shehata and El Damatty (2007, 2008), Darwish and El Damatty (2011), and Aboshosha and El Damatty (2015) indicated the dependency of downburst loads on the event size (i.e., downburst diameter,  $D$ ) and its relative location to the tower of interest, which can be defined by the polar coordinates  $R$  and  $\Theta$  as shown in Fig. 2. This means that in order to estimate the maximum internal forces that can develop in a transmission line system, an enormous number of loading scenarios should be considered. Those loading scenarios should consider the variations in  $D$ ,  $R$ ,  $\Theta$ , and the temporal variation of the downburst velocities. Also, the properties of the transmission line system affect the external wind forces applied on the system as well as the internal forces distribution.



Fig. 1 Guyed tower failure (Hydro One report, 2006)

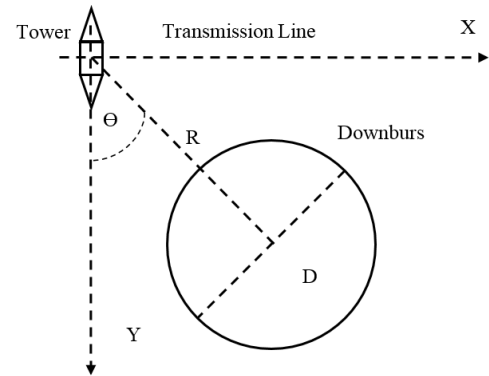


Fig. 2 Downburst characteristic parameters

An extensive research program started and is still going by the authors' research group focusing on studying the response of transmission line structures under downbursts and tornadoes. The research started numerically and then extended recently to include experimental studies such that the one reported by Elawady *et al.* (2017). This research led to the development of a comprehensive and unique computational code, called "HIW-TOWER", which was used by a number of companies in Canada in analyzing transmission line structures under downbursts and in designing them to sustain such events. The program "HIW-TOWER", incorporated the spatial and the time variation of downburst wind field based on the Computational Fluid Dynamics (CFD) simulation conducted by Kim and Hangan (2007) using both the impinging jet and the RANS approaches. This CFD data was validated by comparing the vertical profile of the peak radial velocity to previous experimental simulations (Donaldson 1971 and Didden and Ho 1985) and to an empirical expression (Wood 2001). This CFD data was incorporated into a finite element model (FEM) developed in-house by Shehata *et al.* (2005). The structural part of this numerical model was validated through comparison with bench mark numerical problems reported in the literature. The computer code was then updated by incorporating CFD data based on Large Eddy Simulations (LES) conducted by Aboshosha *et al.* (2015). The advantages of the LES method is that it can model different terrain effects and can also predict turbulence. An experimental program was recently conducted and reported by Elawady *et al.* (2017) at a unique large-scale testing facility, called the WindEEE dome, at the University of Western Ontario, and the results were used to validate the LES simulations developed by Aboshosha *et al.* (2015). Another update of the computer code was conducted by incorporating a semi-analytical approach developed by Aboshosha and El Damatty (2014) for the simulation of the behaviour of the conductors under downburst loading instead of modelling the conductors using finite element modeling. This led to a significant enhancement in the efficiency of the computer code in terms of a reduction in the computational time, since the prediction of the maximum effects of downbursts on transmission line structures requires conducting a large number of non-linear time incremental analyses as will be explained later. Aboshosha and El Damatty (2014) validated their semi-

analytical solution through a comparison with the results obtained from modelling conductors using non-linear finite element code.

It is clear that the validation of the comprehensive computer code was conducted on individual components separately. With the availability of a large-scale testing facility, the WindEEE dome, an opportunity exists to validate the entire numerical code through a comparison with the results of the downburst tests conducted on relatively large-scale aero-elastic model at WindEEE. The validation of the numerical model is not only conducted through comparison between measured and calculated quantities, but also through an assessment for the ability of the model to predict the downburst locations leading to maximum effects on transmission line structures.

The paper starts by providing a brief description of different components of the numerical model. The experiment conducted at WindEEE is then briefly described including the wind field, the tested aero-elastic model, instrumentation, and the test plan. The test results are then presented and used to identify the critical downburst locations causing the maximum line response. The tested transmission line system is then modeled using the previously developed numerical models and comparisons are carried out between the test and the numerical results. The conclusions drawn from the study are then presented.

## 2. Brief about the numerical tools

In this Section, a brief description of the numerical models developed by Shehata *et al.* (2005) and Aboshosha and El Damatty (2014) to analyze transmission lines under downburst winds is provided. Those models can be used to analyze the tower and the conductors under downbursts quasi-statically. Since the downburst field was scaled up to the gust velocity, the quasi-static analysis implicitly considers the background component of the turbulence. The models neglect the resonant response of the towers and the conductors. This was justified in several studies such as Shehata and El Damatty (2007) and Aboshosha and El Damatty (2015) due to the relative high frequency of the tower and the existence of high aerodynamic damping of the conductors which attenuates their vibrations (Holmes 2008, Aboshosha and El Damatty 2015). The experimental study reported by Elawady *et al.* (2017) has shown that the resonant response at high wind speeds does not exceed 20% of the total response. Given the significant uncertainty in the magnitude of the downbursts, this value can be neglected from the practical point of view.

### 2.1 Tower simulation using finite element model (FEM)

This finite element model was developed by Shehata *et al.* (2005) to simulate the tower members. In their model, the tower members were modelled using two noded linear three dimensional frame elements with three translation and three rotation degrees of freedom at each node. A 2-D nonlinear consistent beam element, developed by Koziey

and Mirza (1994) and modified later by Gerges and El Damatty (2002) to include the geometric nonlinear effect, was used to model the conductors. In order to predict accurately the forces transmitted from the conductors to the tower, Shehata *et al.* (2005) recommended to consider three conductor spans on each side of the tower. In addition to the geometric nonlinearity, the model considered the effect of pretension forces, sagging, and the insulator flexibility. Shehata *et al.* (2005) utilized the CFD model developed by Hangan *et al.* (2003) to simulate the spatial and the temporal variations of the mean component of the downburst wind field. The analysis required developing a scaling-up procedure in order to transform the model-scale wind field to full-scale. The scaling procedure involved converting the radial and vertical dimensions of the wind field, the wind speed components and the time, from the model-scale to the full-scale. The conversion approach depends on the assumptions made regarding the full-scale diameter and jet velocity of the acting downburst. This means that the same CFD model was used to produce various downburst events by varying the jet velocity and the diameter of the event. This allowed Shehata and El Damatty (2007) to conduct an extensive parametric study to assess the behaviour of a guyed transmission line system subjected to a generic downburst. The analysis considered permutations between the following variations:

- a. Downburst diameter varying from 500 m to 2000 m.
- b. Distance ratio R/D varying from 0 to 2.2.
- c. Angle of attack  $\Theta$  varying from  $0^\circ$  to  $90^\circ$ .

For each load case, nonlinear analyses considering the entire time history of the wind speeds were quasi-statically conducted for the conductors and the ground wires to evaluate the conductor reactions. The conductor's reactions were then reversed and applied on the tower together with the downburst wind forces acting on the tower members and a linear static analyses were then conducted.

Using the numerical approach, Shehata *et al.* (2005) found that the tower performance against the downburst events is affected not only by the wind intensity but also by the downburst location. Shehata and El Damatty (2007) emphasized on this finding when they identified a unique critical load case that was believed to be the reason of the failure of Manitoba Hydro towers in 1996 (McCarthy and Melsness, 1996). This failure occurred in the cross arm zones. Shehata and El Damatty (2007) reported that this failure occurred under the oblique case of downburst when the touchdown point of the downburst was located at an angle of attack ranging between  $15^\circ$ ~  $45^\circ$  measured from the tower of interest. Although Shehata *et al.* (2005) model was able to study the behaviour of the transmission line system using the extensive parametric study, the model was computationally expensive. This was mainly due to the iterative nonlinear analysis required for the conductors. This motivated Aboshosha and El Damatty (2014) to develop a semi-analytical technique to analyze the conductors as explained in the next section.

## 2.2 Conductors semi-analytical technique

Aboshosha and El Damatty (2014) developed a semi-analytical closed form solution to accurately and efficiently analyze multi-spanned conductors when subjected to downburst loads. The model required solving a set of equations to estimate the unknown displacements at the insulator-conductor connection points. By limiting the unknown displacements to degrees of freedom at the conductor's supports, a significant reduction in the computational time was achieved compared to nonlinear finite element analysis. The technique is able to determine the response under non-uniform loads in both the lateral and vertical directions which taking into account the insulator's flexibility, and pretension force in the conductors. Aboshosha and El Damatty (2014) derived six equations to solve the six unknowns (three displacements and three reactions) at the conductor-insulator points by considering the following: two equations resulting from the moment equilibrium of the conductors, one equation resulting from equating the conductor length with the integral of the deformed curve, and three equations resulting from the moment equilibrium of the insulator. The initial displacements were assumed first, then the reactions  $R_y$  (transverse direction) and  $R_z$  (vertical direction) were updated. This was followed by solving for the reaction  $R_x$  (longitudinal direction) and  $d_x$  (longitudinal displacement) iteratively, then updating the displacement components  $d_x$ ,  $d_y$  and  $d_z$ . The whole process is repeated until convergence occurs. This technique showed superior performance (around 180 time faster) when compared to finite element analysis of transmission lines conductors. More details about the technique can be found in Aboshosha and El Damatty (2014).

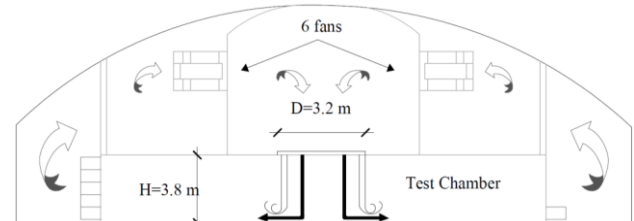
## 3. Wind tunnel testing at WindEEE

### 3.1 Downburst wind field

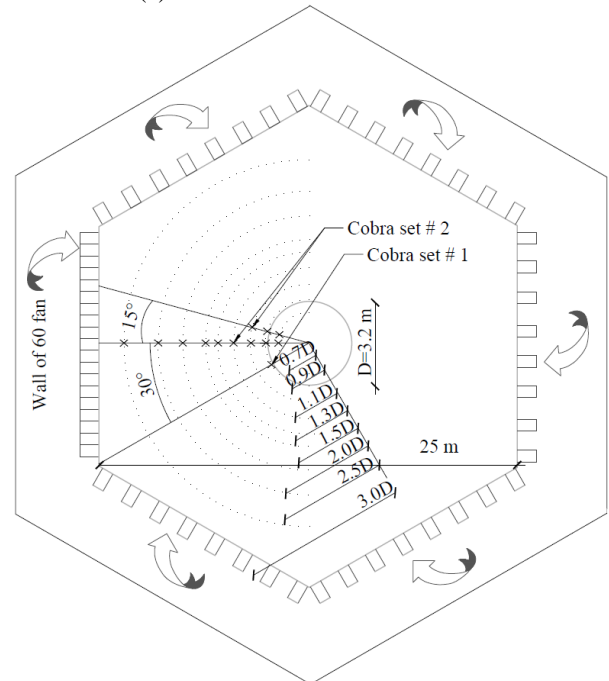
The WindEEE dome is utilized to simulate a lab-scale downburst. WindEEE has a hexagonal testing chamber with a maximum width of 25 m and a height of 3.8 m as shown in Fig. 3. Along the perimeter of the testing chamber, 100 reversible fans exist to produce large scale wind profiles. To produce high intensity wind fields such as tornadoes and downbursts, the chamber is attached to an upper plenum supplied by 6 fans and a circular nozzle called the bell mouth.

To form a downburst with a chosen intensity, the air inside the upper plenum is pressurized by running the upper plenum fans together with the fans mounted on the walls of the testing chamber with a specific electricity power, then the bell mouth is opened suddenly to release the air from the upper plenum to the testing chamber. The released air impinges towards the ground of the test chamber and forms the downburst. The diameter of the bell mouth  $D$  is chosen to be 3.2 m, which leads to a height to diameter ratio of 1.2. Such a ratio is within the typical height to diameter  $H/D$  ratios of a real downburst that was reported to be between

1.0~4.0 (Hjelmfelt 1988). Fig. 4 shows the formation of the downburst at the WindEEE dome. After the downburst is formed, it interacts with the roughness elements placed on the floor of the test chamber. These roughness elements can be controlled automatically to represent various terrain exposures. In the current study, the roughness element size is selected to be 0.15 m to simulate the open terrain exposure.



(a) Elevation WindEEE chamber



(b) Plan view of WindEEE chamber

Fig. 3 Testing chamber



Fig. 4 Downburst formation snapshot at WindEEE



Fig. 5 Wind Field measurement using cobra probe devices

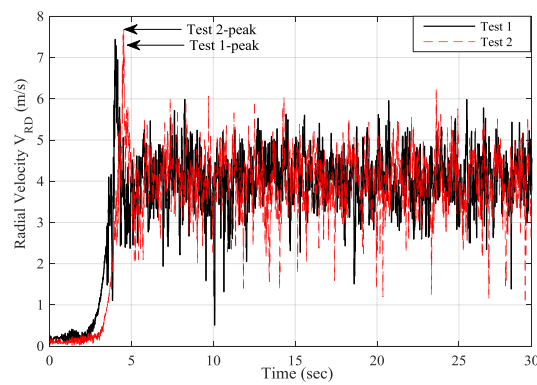


Fig. 6 Repeatability of the downburst wind field

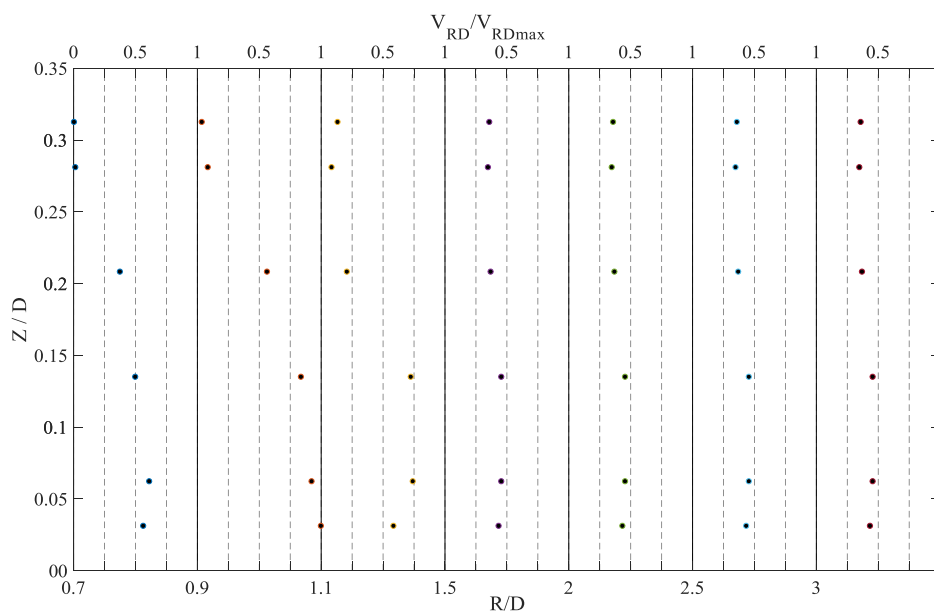


Fig. 7 Evolution of downburst radial profiles at time = 4.84 seconds

The downburst wind field at the WindEEE dome is measured at various angles and radii relative from the center of the downburst to assess the homogeneity of the flow and to evaluate the variation of the wind field with the change of the distance from the center of the touchdown

point of the downburst. The flow field is measured using two sets of cobra probes with a sampling frequency of 156 Hz. Each cobra probe set consists of six three-dimensional probes mounted on a column at heights of 0.1, 0.2, 0.43, 0.67, 0.9, 1.0 m. Fig. 3 shows the selected locations of the

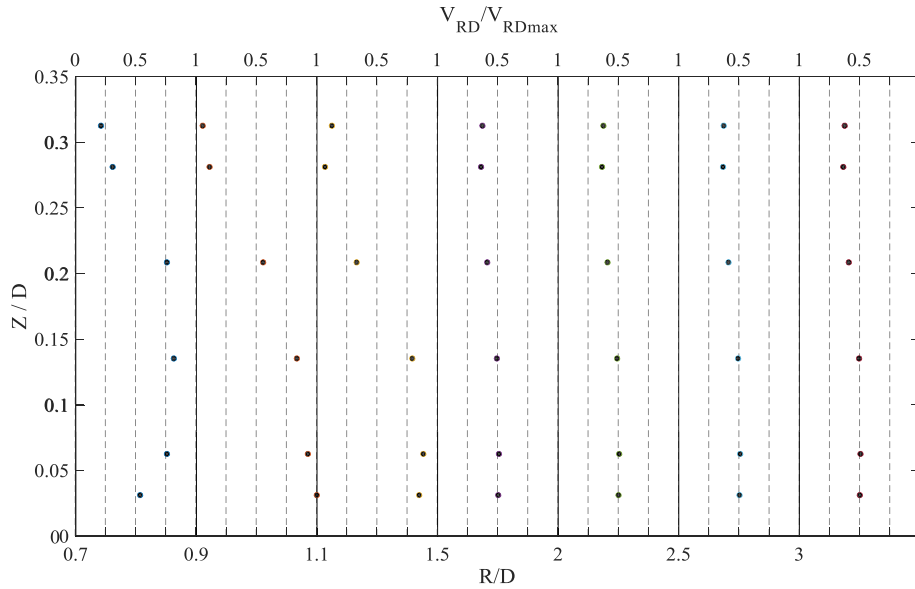


Fig. 8 Instantaneous of radial wind profiles

cobra probe sets while Fig. 5 shows a typical probe set. During the measurements, one set is always located at a radius of  $0.9D$  and an angle of  $-30^\circ$ , where the angle is measured from the line passing through the center of downburst perpendicular to the wall of the main fans assuming positive sign for clockwise direction, while the other set is movable. The movable probe set is placed at radii of  $0.7D$ ,  $0.9D$ ,  $1.1D$ ,  $1.3D$ ,  $1.5D$ ,  $2.0D$ ,  $2.5D$ , and  $3.0D$  at an angle of  $0^\circ$  as well as radii of  $0.7$ ,  $0.9$ ,  $1.1$  at an angle of  $+15^\circ$ . This is done to correlate between the time histories of the radial velocity resulting from different events. The measured speeds recorded from the two cobra sets are correlated by unifying the time instance corresponding to the peak happening at probe set no. 1 for different downburst simulations. An example of the time history of the radial velocity,  $V_{RD}$ , is shown in Fig. 6. The figure shows  $V_{RD}$  at a point of  $X=0$  m and  $Y=2.88$  ( $R=0.9D$ ) measured from the downburst center at a height of  $Z=0.2$  m. The velocity measurement at this point is recorded twice for two different downburst simulations, labeled test 1 and test 2 in Fig. 6, to ensure that the test is repetitive. The figure shows a minor difference of 3% between the peak radial velocities recorded for the two downburst simulations which means the test is reasonably repeated. The time shift between the peaks of the two tests, Test 1 and Test 2 in Fig. 6, is expected since the time instant of opening the bell mouth and the time instant of recording the velocity are manually controlled. Downburst wind velocities are processed and decomposed into mean and fluctuating components. The mean component of the velocity is usually named as “running-mean” or the “non-stationary mean” as a result of the time dependency of the downburst velocities (Choi and Hidayat 2002, Holmes *et al.* 2008, Kwon and Kareem 2009). The running mean wind speed of the downburst is extracted using the approach described by Aboshosha *et al.* (2015)

and explained and validated by Elawady *et al.* (2017). The mean radial velocities are extracted from the measured wind field for the measured radii distances. Fig. 7 shows the evolution of the vertical profile of the mean radial velocities, normalized to the maximum value of  $V_{RD}$ , for the different  $R/D$  ratios for an open terrain. The figure is developed at the time instant, 4.84 sec (model-scale), corresponding to the maximum radial speed measured in the entire wind field which is found to take place at  $R=0.9D$  and  $Z=0.03$ .

Fig. 8 shows the instantaneous vertical profiles of the mean  $V_{RD}$  normalized to the maximum mean  $V_{RD}$  for distance ratios of  $R/D$  equal 0.7 to 3.0. More information regarding the wind field is discussed by Elawady *et al.* (2017).

### 3.2 Aero-elastic transmission line model

A brief description of the full scale transmission line system followed by a description of the aero-elastic model and a summary of the instrumentation employed to acquire the test measurements is provided. More information can be found in Elawady *et al.* (2017).

#### 3.2.1 Full-scale transmission line system

The current study utilizes the aero-elastic transmission line designed and reported by Elawady *et al.* (2017) which consists of seven towers as shown in the test layout provided in Fig. 9. A three-dimensional perspective of the line tower is shown in Fig. 10. The global axis system used in the current study is shown in Fig. 10 where the X-axis represents the direction of the transmission line, the Y-axis is the direction perpendicular to the line direction, and the Z-axis is the vertical direction. The tower is supported by 4 guys and carries three conductor bundles at the insulators;

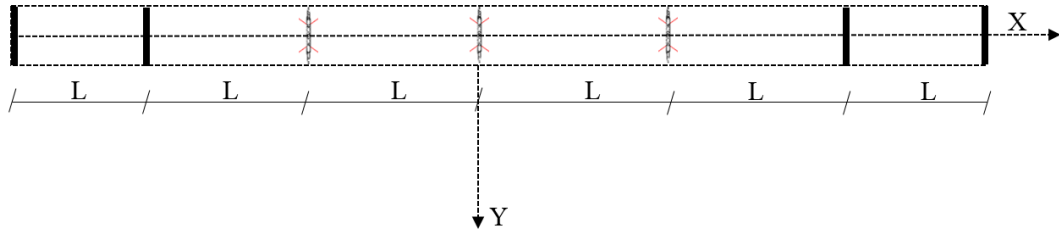


Fig. 9 Schematic of the test layout

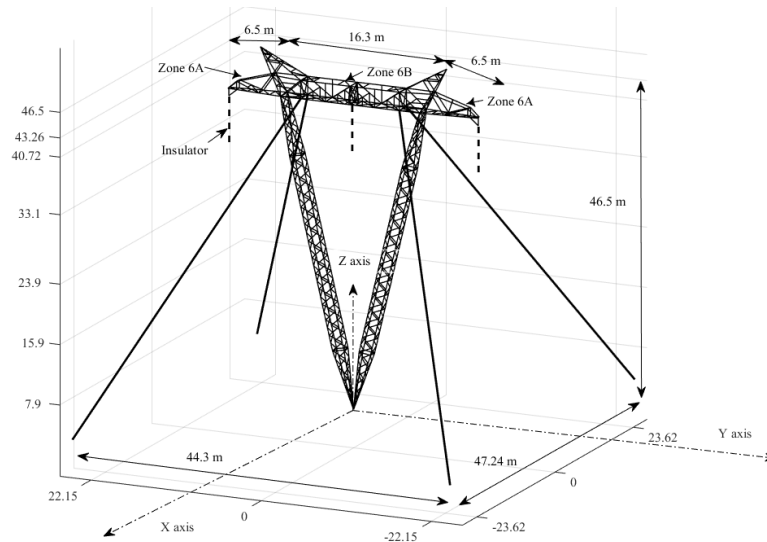


Fig. 10 3-D view of the prototype tower

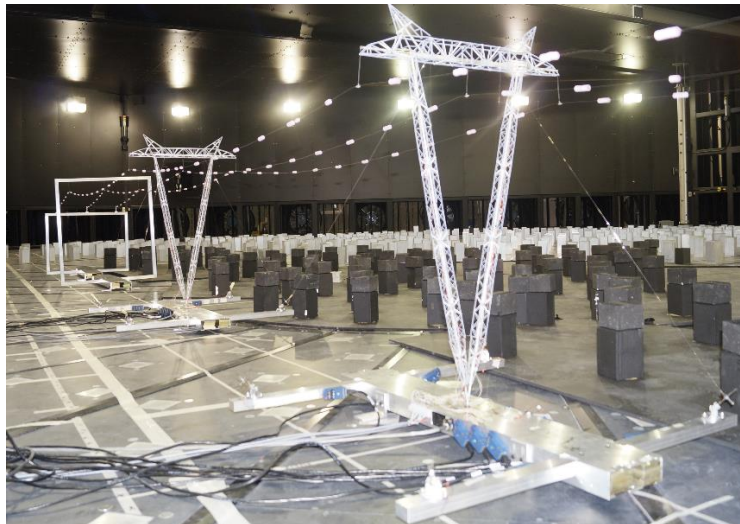


Fig. 11 Half-length of the assembled line

two at the tip of each cross arm and one at the center point of the main girder. Two span cases are considered in the current test;  $L = 125$  m or  $250$  m with a sag at the mid-span of  $3.25$  m or  $6.5$  m, respectively. Although this is less than the typical span length used for such towers (i.e.,  $\sim 200$ - $500$  m), it is still practical and it represents the spans used in

some cases. A pretension force of  $11$  kN is applied to all the guys. The tower is resting on the ground on a hinged support that allows the rotations at the tower center while preventing the displacements. Fig. 11 shows a photo of the tested line.

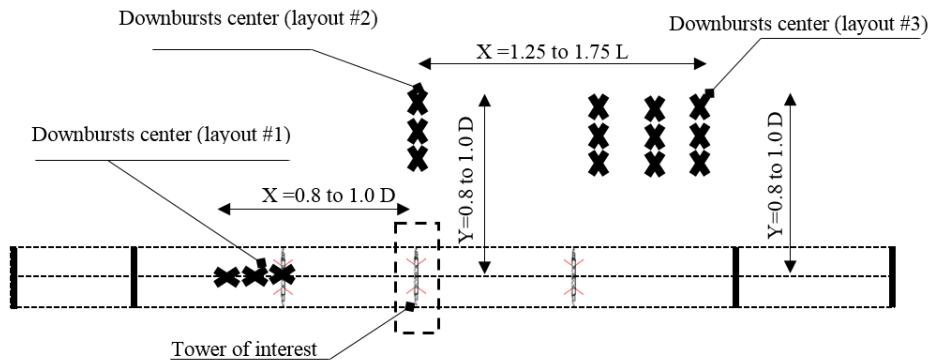


Fig. 12 Summary of downburst-structure orientations for the considered layouts

### 3.2.2 Aero-elastic modelling of the line system

The aero-elastic model is constructed at a length scale of 1:50 and a velocity scale of 1:7.07. The scaling ratios of all other forces and stiffness are given in Elawady *et al.* (2017). The model of a single tower, such as towers A to C in Fig. 9, is comprised of the following components: a) an aluminum spine designed to model the lateral and torsional stiffness of the tower system, b) non-structural sections made of plastic, referred to as cladding, attached to the spine to obtain the correct distribution of masses and drag forces. Dimensions of the aluminum spine and the conductors are given By Elawady *et al.* (2017). The conductor bundle is simulated using a steel wire in addition to discrete aerodynamic drag elements to simulate the mass and the drag of the conductor bundle as shown in Fig. 11. The stiffness of the insulators is represented by steel rod as shown in Fig. 11. The spans of the aero-elastic line considered in the current study are 5 m and 2.5 m representing a full-scale spans of 250 m and 125 m, respectively. This means that the span to diameter ratio  $L/D$  is equal to 1.5 to 0.7, respectively.

The boundary condition of the line is satisfied using a two-degree of freedom gimbal system, 2D Universal Base Support, at the tower center together with the four guys. The intermediate support of the conductors is modeled using the insulator rod with proper flexibility. At the end of the line, the conductors are attached to rigid frames.

### 3.2.3 Instrumentations and data acquisition system

Different instruments are used to measure the line responses. Those instruments include: strain gauges to measure in-plane (Y direction) and out-of-plane (X direction) mid-height moments at the two legs ( $M_{i1}$  and  $M_{i2}$ , respectively) and out-of-plane cross arm moment ( $M_{Ca}$ ), strain gauges to measure the tension in the guys ( $T_{Guy}$ ), and force balance to measure the center point forces in three principal directions. This allows to estimate the base shears ( $Q_X$  and  $Q_Y$ ) and the base moments ( $M_{Xb}$  and  $M_{Yb}$ ) as per the following expressions:

- Base shear =  $\Sigma$  Guys force in direction of interest + center support force in the direction of interest.
- Base moment =  $\Sigma$  Guys force in direction of

interest  $\times$  lever arm measured from the guy's support to the center support in the direction of interest.

### 3.3 Experimental test plan

The test configurations and layouts are selected in view of the findings of the previous numerical studies (Shehata and El Damatty 2007 and Darwish and El Damatty 2011) together with the characteristics of the measured downburst field. Regarding the radial distance corresponding to the peak radial velocity, the results show that the maximum radial speed occurs at a radial distance  $R \approx 0.9 D$ . Therefore, in the current study, the tower of interest is placed at three different radial distances around the location of the peak radial velocity; i.e.,  $R = 0.8, 0.9$ , and  $1.0 D$ . In addition, the current study considers three orientations of the downburst with respect to the tower;  $\Theta = 0^\circ, 90^\circ$ , and a number of intermediate oblique cases. Regarding the selection of the line span, the following is considered: 1) at  $\Theta = 90^\circ$ , Shehata and El Damatty (2007) showed that no conductor forces exist, therefore, only a single tower is considered; 2) at  $\Theta = 0^\circ$ , Shehata and El Damatty (2007) showed that the maximum lateral loads acting on the line occur when the downburst diameter is small, i.e., at high  $L/D$  ratios. Therefore, a span of 5 m is considered for the angle of attack of  $\Theta = 0^\circ$ ; 3) at  $0^\circ < \Theta < 90^\circ$ , Shehata and El Damatty (2007) reported high longitudinal force developing in the conductors when the ratio  $L/D$  is less than unity. Therefore, for the oblique configurations of the downburst loads, a span of 2.5 m is considered which leads to an  $L/D$  equal to  $\sim 0.7$ .

Three layouts (see Fig. 12) are considered in the current study to assess the tower responses under different configurations of the downburst. Table 1 summarizes the considered layouts and the parameters used in the test. The table shows the location (X and Y distances) of the middle tower (the tower of interest) with respect to the downburst touchdown point for each layout. The towers are tested under a peak radial speed of 8 m/s model-scale, corresponding to a radial speed of 56 m/s full-scale, for an open terrain exposure. The next section describes each of the studied layouts in details.

Table 1 Test layouts

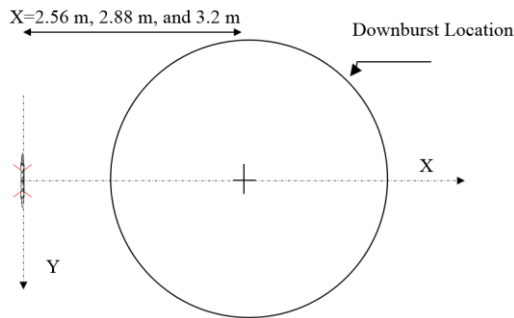
Layout no.	$\Theta$ (degree)	Middle tower location			Line span (m)	No. of spans
		X (m)	Y (m)	R/D		
1	90°	2.56, 2.88, 3.2	0	0.8, 0.9, 1.0	-	-
2	0°	0	2.56, 2.88, 3.2	0.8, 0.9, 1.0	5	4
3	44° to 60°	3.125, 3.75, 4.375	2.56, 2.88, 3.2	1.26, 1.48, 1.7	2.5	6

**3.3.1 Layout 1: Maximum longitudinal loads (Angle of attack of 90°)**

In this layout, a single tower is considered in the test where no conductors are attached. The tower is placed such that the downburst winds act on the tower face perpendicular to the line direction (X-direction). A schematic of this layout is provided in Fig. 13(a) showing the locations of the tested tower relative to the downburst center. The figure shows that the tower is placed at longitudinal distances  $X = 2.56$  m,  $2.88$  m, and  $3.2$  m from the center of the downburst. This is corresponding to distance ratios  $R/D = 0.8, 0.9,$  and  $1.0,$  respectively. Fig. 13(b) shows a picture for test layout 1 inside WindEEE.

**3.3.2 Layout 2: Maximum transverse loads (Angle of attack of 0°)**

In this layout, the tower is placed such that the downburst winds act on the transverse direction, Y direction, of the line. The layout considers four line spans each of 5 m.



(a) Schematic plan view of layout 1



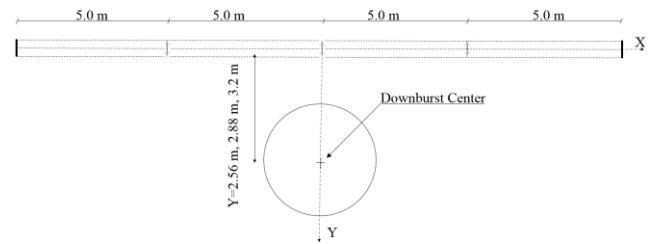
(b) Layout 1 testing at WindEEE

Fig. 13 Test layout 1

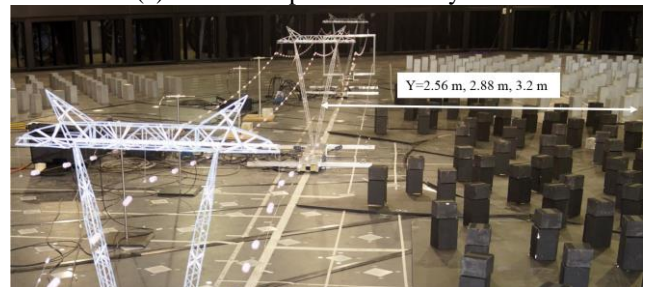
This is because the total width of WindEEE is 25 m, so two spans were removed only in this layout in order to accommodate the line with 5 m span. Fig. 14(a) shows the location of the middle tower with respect to the downburst center at the testing chamber. The tower is placed at a transverse distances Y equal to 2.56 m, 2.88 m, and 3.2 m corresponding to a distance ratio R/D equal 0.8, 0.9, and 1.0, respectively. Fig. 14(b) shows a picture for test layout 2 inside WindEEE.

**3.3.3 Layout 3: Maximum oblique loads (Yaw angles of attack)**

This layout examines the tower response when the downburst acts with an oblique angle on the line. Fig. 15(a) shows the considered locations of the middle tower of the line with respect to the downburst center while Fig. 15(b) shows a picture for test layout 3 inside WindEEE. Nine tower locations are selected representing the permutations of distance ratios (R/D) equals 0.8, 0.9, and 1.0 in Y direction and a distance to span ratio (X/L) of 1.25, 1.5, and 1.75 in X direction.



(a) Schematic plan view of layout 2



(b) Layout 2 testing at WindEEE

Fig. 14 Test layout 2

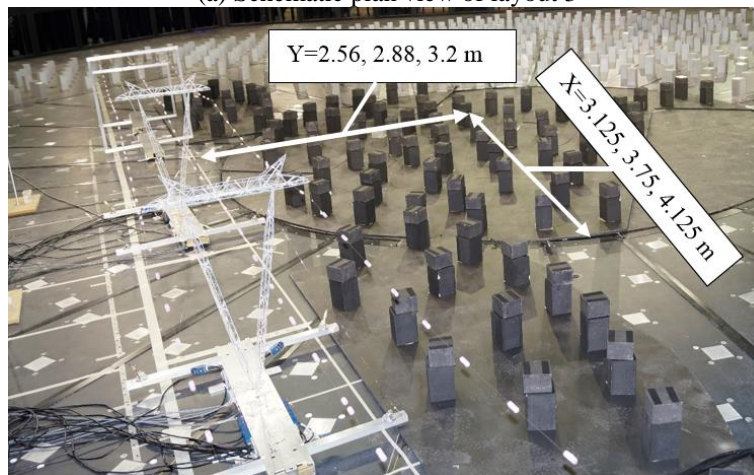
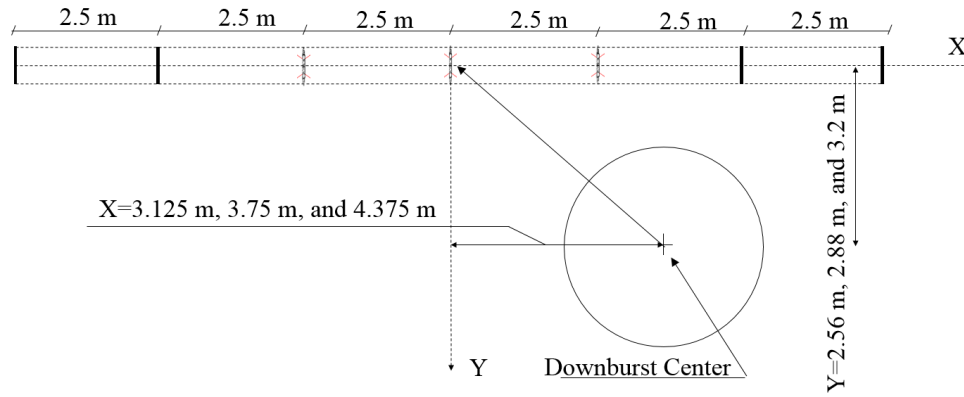


Fig. 15 Test layout 3

#### 4. Variation of peak and mean responses of the aero-elastic model with the downburst location

This section discusses the tower responses for the three studied layouts in view of the measured base shears ( $Q_X$  and  $Q_Y$ ), base moments ( $M_{Xb}$  and  $M_{Yb}$ ), mid height moments ( $M_{Xi}$  and  $M_{Yi}$ ), and cross arm moment ( $M_{Ca}$ ). The section aims at examining the findings of discussed numerical studies that indicated high dependency of the tower responses on the location of the downburst event.

Fig. 16 shows a sample of the peak and the mean time history responses of the tower for layout 1 when the tower is located at a distance ratio  $R/D = 0.9$  under a peak radial velocity of 8 m/s, where  $M_{Xb}$  is the base moment measured in the X direction,  $Q_X$  is the base shear measured in the X direction,  $T_{Guy}$  is the net tension force measured in the guys due to downburst loads, and  $M_{Xi}$  is the mid-height moment measured in the X direction at the right leg of the tower (the leg closer to the touchdown point of the downburst).

The mean component of the structural responses is separated from the measured peak response, using the filtering function described by Elawady *et al.* (2017), as shown in Fig. 16. The figure shows that a sudden peak of the response occurs in a very short period of the entire time history. Then, the response decreases suddenly till reaching a minimum value.

The maximum peak and the maximum mean responses obtained from each of the three tested layouts are shown in Fig. 17 to 20. The figures show the variations of the base shears,  $Q_i$ , mid-height moments at the two legs,  $M_{i1}$  and  $M_{i2}$ , base moments,  $M_{ib}$ , and cross arm moment,  $M_{Ca}$ , with the distance ratio  $R/D$ , the angle of attack  $\Theta$ , and the type of response; i.e., peak and mean responses.

##### 4.1 Layout 1: Maximum longitudinal loading ( $\Theta=90^\circ$ , Fig. 17)

Generally, it is found that peak responses occur at  $R/D$  ranging between 0.8 to 0.9; i.e.,  $X = 2.56$  m to 2.88 m. For example, the maximum cross arm and base moments occur at  $R/D = 0.8$ , while the maximum mid-height moment and base shear occur at  $R/D = 0.9$ . Both the base moment and the cross arm moments are more sensitive to the wind forces acting on the cross arm level, which are maximum when downburst center is located at  $R/D \sim 0.8$  as shown in Fig. 8.

The base shear and mid-rise moment are more sensitive to the loads acting on the legs of the tower, which are maximum when  $R/D = 0.9$ . Fig. 17 shows that the mid height moment  $M_{X1}$  is approximately equal to that of  $M_{X2}$  since both tower legs are exposed approximately to equal wind pressure.

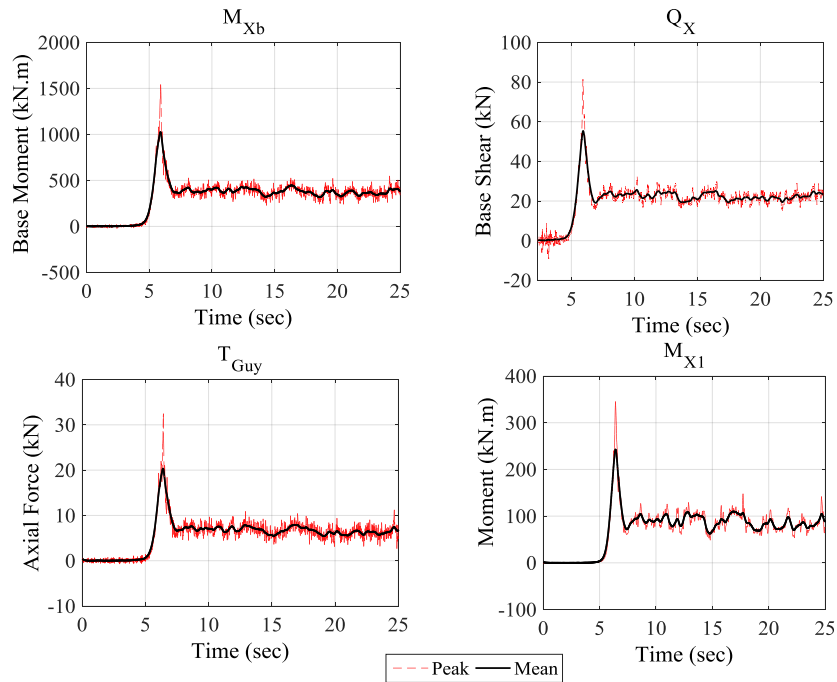


Fig. 16 Sample response of the middle tower subjected to downburst loads

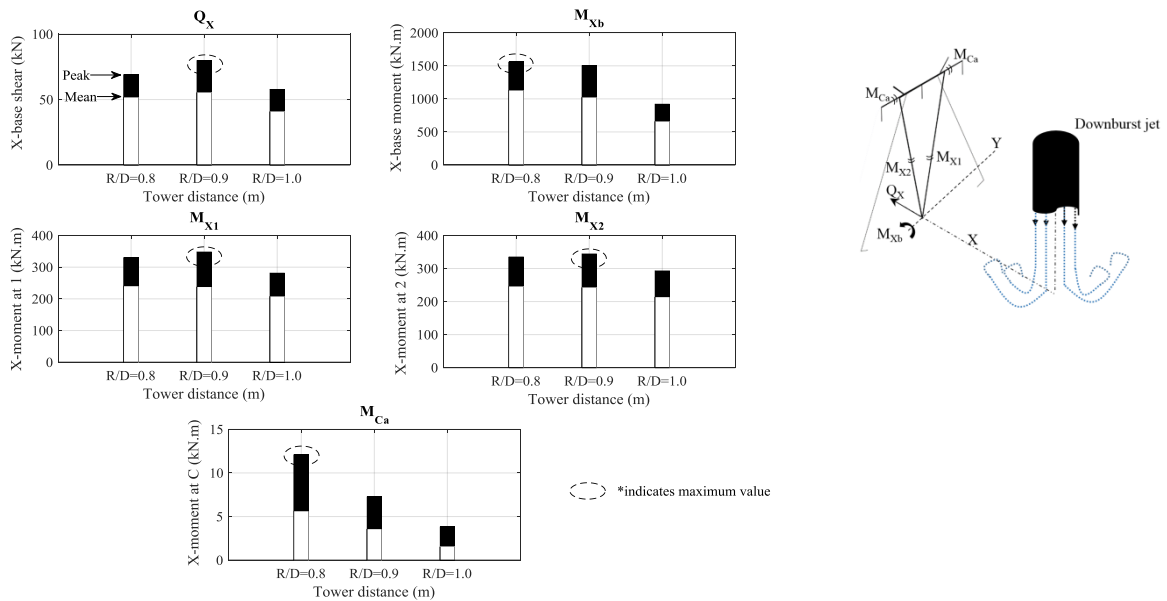


Fig. 17 Layout 1 maximum peak responses of the tower B

4.2 Layout 2: Maximum transverse loading ( $\Theta=0^\circ$ , Fig. 18)

The test results show that the maximum base shear, base moment, and mid height moment occur when the middle tower is placed at a distance ratio  $R/D = 0.9$ . This corresponds to a distance ratio  $R/D = 0.8$ . At  $R/D = 0.9$ , the responses are slightly less than that of  $R/D = 0.8$ . The mid height moment  $M_{Y1}$  is less than  $M_{Y2}$ . The ratio  $M_{Y1}/M_{Y2}$  is found to be equal to 0.73, 0.8, and 0.67 for  $R/D$  of 0.8, 0.9, and 1.0, respectively.

4.3 Layout 3: Maximum oblique loading ( $\Theta=0^\circ$ , Fig. 19 and 20)

The results show that the maximum base shears, mid height moments, and out-of-plan cross arm moment occur when the middle tower is placed at a distance  $X = 3.125$  m and  $Y = 2.56$  m. On the other hand, the maximum base moments occur when the middle tower is placed at a distance of  $X = 3.75$  m and  $Y = 2.88$  m.

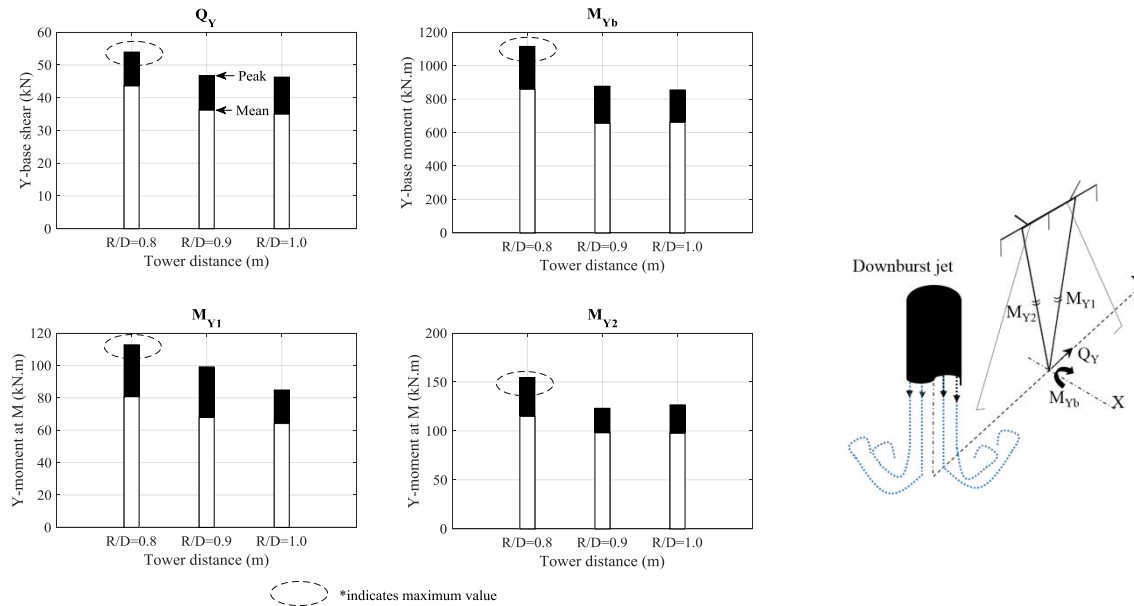


Fig. 18 Layout 2 maximum peak responses of the tower B

Both cases correspond to the application of the maximum downburst speed (at  $R = 0.8\sim 0.9 D$ ) on the second line span adjacent to the tower of interest (1.25-1.5  $L$ ). This is in an agreement with the findings of Shehata and El Damatty (2008) where the critical configuration causing the maximum longitudinal force in the conductors is found at  $R = 1.6 D$ ,  $\Theta = 30^\circ$ , and  $L/D = 0.5$  to  $0.8$  which leads to a projection of the downburst center on the second span of the line measured from the tower of interest. It is also found that the base responses in the two principal directions, X and Y, are in the same order, which can be attributed to the fact that the incoming angle of attack at the tower of interest is close to  $45^\circ$ . The ratio between the conductor longitudinal to transverse reactions is found to be in the order of 58% where the longitudinal force is calculated by analyzing the cross arm moment measured in the test and the transverse force is calculated using the ASCE-74 (2010) wind force equation; i.e.,  $transverse\ force = 0.5p (V_{RDC})^2 d L$ , where  $V_{RDC}$  is the radial velocity of the downburst at the conductor's level,  $d$  is the conductor's diameter, and  $L$  is the conductor's span.

The comparison between the peak response values obtained from the three tested layouts shows the followings:

- Base response in layout 1 is approximately 40% larger than that in layout 2, and also mid-height leg moment in layout 1 is almost double that in layout 2 although no conductor's loads exist in layout 1. This is attributed to the large tower projected area in the wind direction in layout 1 compared to that in layout 2.
- The cross arm moment induced from layout 3, due to the contribution of the longitudinal force developing in the conductors, is 1.7 times larger than that induced from layout 1 resulting from applying the wind loads orthogonally on the cross arm. This ratio may significantly increase

with the increase of the span length, the wind intensity, or the change in the conductor's properties (Aboshosha and El Damatty 2015b).

Those observations agree with the findings of the previous numerical studies. The test results highlight that the tower response is sensitive to the location of the touchdown point of the downburst. The results also show that a downburst location may be critical for a specific zone of the tower not all the tower zones in general. Therefore, a special attention should be taken into consideration when designing the transmission line systems to resist a generic downburst load where several loading scenarios should be considered. In the following section, the running mean wind speeds decomposed from the measured downburst wind field, reported earlier in this study, are implemented in the numerical models, described earlier in this study, to estimate the corresponding running mean responses of the tower and consequently validating the numerical models.

## 5. Results obtained from the numerical models

The built in-house numerical models are validated by comparing their aerodynamic forces, conductor reactions, and the distribution of the straining actions to those measured during the test. The wind velocities used in the numerical models to simulate the wind loads are extracted from the cobra probe measurements of the downburst simulation conducted at WindEEE as described earlier in this paper. This is to provide the numerical models with wind pressures similar to those applied on the tested transmission line. The validation process considers evaluating the accuracy of the numerical models in estimating both the mean and the peak responses.

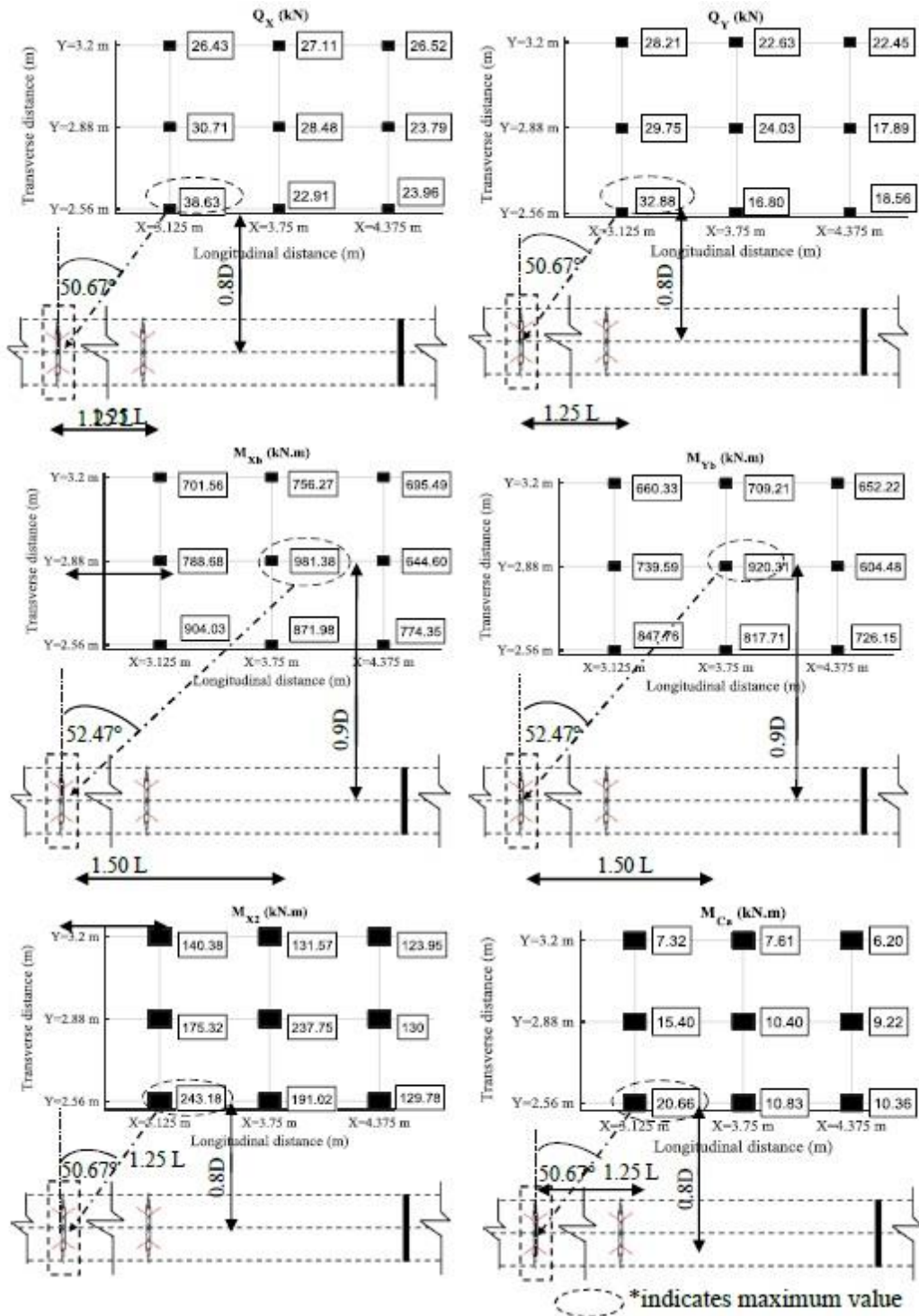


Fig. 19 Layout 3 maximum peak responses of tower B

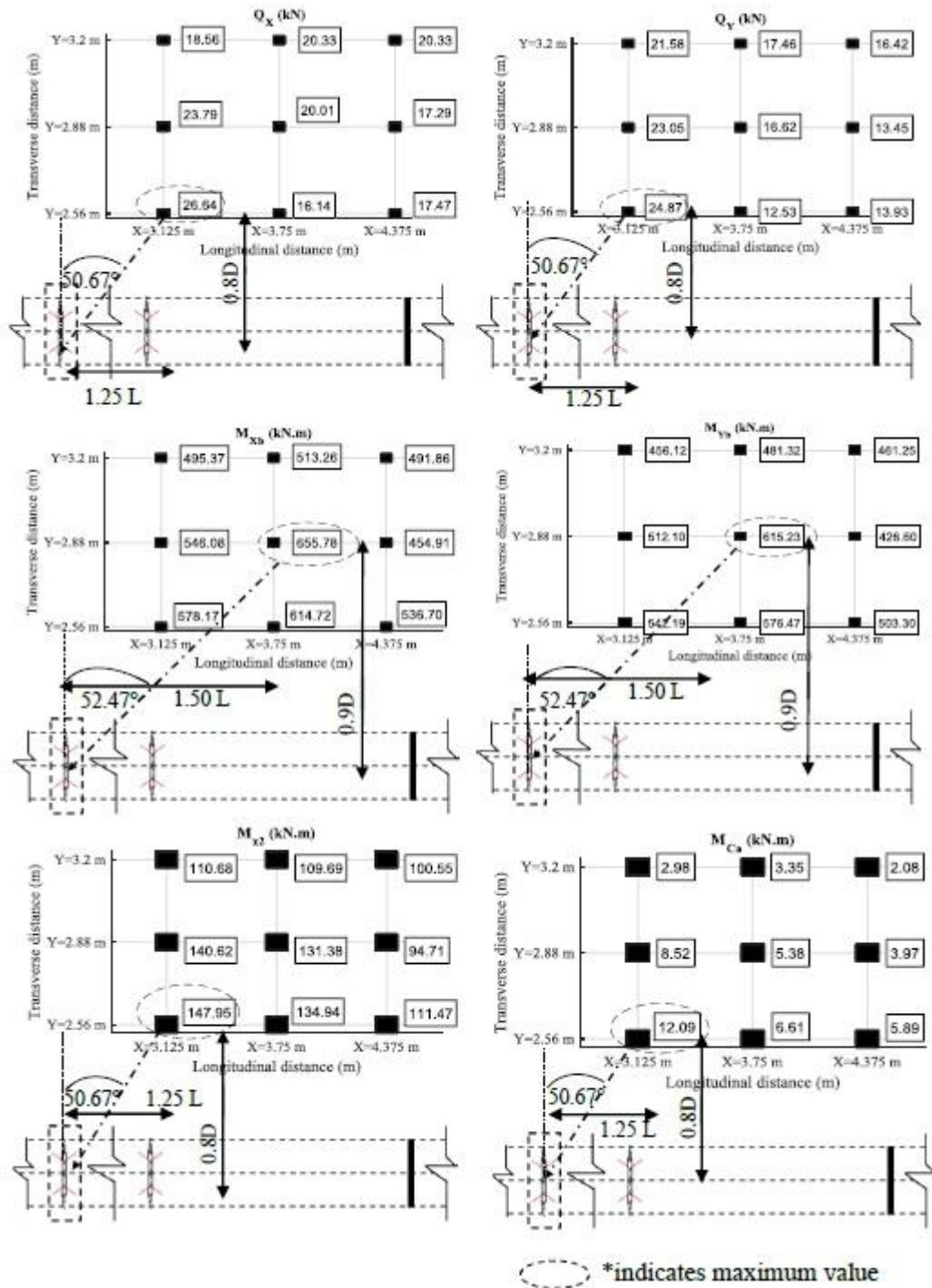


Fig. 20 Layout 3 maximum mean responses of tower B

Table 2 Selected test cases for validating the numerical models

Case	Validation case # 1	Validation case # 2	Validation case # 3	Validation case # 4
Layout	1	2	3	3
Location	X=2.88 m Y=0 m	X=0 m Y=2.56 m	X=3.125 m Y=2.56 m	X=3.125 m Y=2.88 m
Span	Single tower	5 m	2.5 m	

First, the mean component of the downburst wind field is implemented in the numerical models to validate the solution of the numerical models without the effect of the turbulence and consequently the dynamic response of the system. Second, the peak wind velocities of the downburst are implemented in the numerical models in order to assess the accuracy of the quasi-static solution assumed in the numerical models. Four test cases are selected for the validation process as summarized in Table 2: (i) one case from layout 1 (longitudinal case), (ii) one case from layout 2 (transverse case), and (iii, iv) two cases from layout 3 (Oblique cases). These chosen cases are found critical and responsible for the maximum responses as indicated in Fig. 17 to 20.

The validation of the numerical models is conducted at three levels: (i) at the level of the external forces (aerodynamics) by comparing the base moments and the base shears, (ii) at the conductor level, by comparing the out-of-plane cross arm moments and (iii) at the level of distributing the straining actions, by comparing guy's tensions, center support horizontal forces, mid-height moments.

### 5.1 Validation of the external forces evaluation

In this section, a case from Layout 1, Validation case #1 (layout 1-longitudinal load case), is first selected to check the accuracy of the numerical models in calculating the external forces applied on the tower members while eliminating the conductors effect. Another case is selected from Layout 2 (transverse load case), Validation case #2, which represents the maximum transverse loads acting on both the tower and the conductors. Table 3 shows a comparison between the base shears and base moments obtained from the experiment and the numerical models for validation cases #1 and #2. The comparison considers both the maximum mean and the maximum peak responses of the tower. For the maximum mean responses, the maximum difference is found to be equal to 6% in Validation case #1 and 13.5% in Validation case #2. On the other hand, the maximum difference between the test and the numerical model in the case of the maximum peak responses results is found to be -0.6% for validation case # 1 and 22% for validation case # 2.

### 5.2 Validation of the conductor response

As discussed earlier, the oblique case of the downburst loading results in a nonlinear longitudinal force,  $R_x$ , developing in the conductors and causing an out-of-plane bending moment on the cross arm zone of the transmission

line system as illustrated in Fig. 21. Two cases are selected out of the described test cases to examine the efficiency of evaluating  $R_x$  using the built in-house semi analytical technique developed by Aboshosha and El Damatty (2014). Those two cases are responsible for the largest  $R_x$  in the conductors and consequently the largest  $M_{Ca}$  in the cross arm zone. Those two cases are described in this section as validation cases #3 and 4. An excellent agreement is found in the two studied cases as shown in Table 4 with a maximum difference of 5% for the maximum mean response cases. The discrepancy increases in the case of the maximum peak response cases as shown in the table where the maximum difference reaches 20%.

### 5.3 Validation of straining action distributions

The third part of the validation process investigates the ability of the numerical model developed by Shehata *et al.* (2005) to estimate the right stiffness of the structure zones and consequently compute the distribution of the straining actions accurately. This is examined by comparing the guy's tensions, center support's reactions, and mid height moments obtained from the numerical models to those measured during the test. Validation cases #1, 2, and 3 are used to examine the numerical model solutions for different angles of attack. Table 5 shows a comparison between the guys tensions, the center support force, and the mid height moment obtained from the WindEEE testing to those obtained using the numerical models for both the mean and the peak responses. For the mean responses, the analyses show that the guy tensions, the center support reaction, and the mid-height moment estimated using the aero-elastic testing and the developed numerical models are in a good agreement with a maximum difference of 12%, 16% and 10%, respectively. The discrepancies found in the peak responses are higher where a maximum error of 25% is observed.

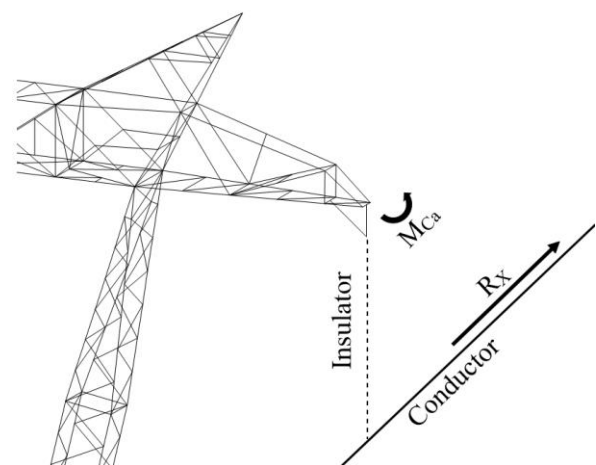


Fig. 21 Free body diagram of the cross arm system under the oblique case

Table 3 External forces validation

		Base Shear (kN)			Base Moment (kN.m)		
		Test	Numerical model	% Difference	Test	Numerical model	% Difference
Validation Case # 1	Mean	55	58.3	5.91	1025	1005.5	1.9
	Peak	79.9	80.3	0.6	1505	1403	6.8
Validation Case # 2	Mean	43.6	37.4	10.4	858.5	742.6	13.5
	Peak	53.9	43.5	19.4	1115	868	22.1

Table 4 Conductor model validation

		R <sub>x</sub> (kN)		
		Test	Numerical model	% Difference
Validation Case # 3	Mean	12.1	11.8	2.5
	Peak	20.7	16.9	18.1
Validation Case # 4	Mean	8.5	8.1	5.1
	Peak	15.4	12.3	20.2

Table 5 Straining actions distribution validation

		Guy tension (kN)		
		Test	Numerical model	% Difference
Validation Case # 1	Mean	10.90	11.00	0.92
	Peak	19.71	18.50	6.15
Validation Case # 2	Mean	9.50	8.85	6.84
	Peak	15.03	13.16	12.43
Validation Case # 3	Mean	9.65	10.84	12.31
	Peak	14.48	14.63	1.08
Center support force (kN)				
		Test	Numerical model	% Difference
Validation Case # 1	Mean	44.1	37.3	9.0
	Peak	60.1	60.9	1.4
Validation Case # 2	Mean	34.1	27.2	10.1
	Peak	38.9	32.8	15.5
Validation Case # 3-X	Mean	27.8	15.0	16.3
	Peak	38.9	29.3	24.7
Mid height moment (kN.m)				
		Test	Numerical model	% Difference
Validation Case # 1	Mean	242.5	218.3	10.0
	Peak	344.5	288.3	16.3
Validation Case # 2	Mean	80.7	74.2	9.8
	Peak	112.7	95.5	15.2
Validation Case # 3-X	Mean	148.0	162.3	-9.7
	Peak	243.18	240.0	1.3

It is observed that higher difference exists in the validation cases where the conductors are contributing to the tower response causing extra forces. This may be attributed to the uncertain aerodynamics of the circular sections tested in wind tunnel experiments. Another source of error is the accuracy of interpolating the wind field in the locations that were not measured in this study. The observed increase in the error in the case of peak responses comparison is believed to be due that the numerical models adopt only the quasi-static response while ignoring the resonance response.

## 6. Conclusions

An aero-elastic model of a multi-spanned transmission line system is utilized to validate two numerical models that were previously developed in-house to evaluate the response of transmission line systems under downburst loads. The aero-elastic transmission line model consists of three aero-elastic towers and other four rigid frames to simulate a total number of six spans. The downburst wind field simulated at the WindEEE Research Institute is measured in space and validated. The desired geometric scale is selected to be 1:50. A brief description the procedures and assumptions of the design of the aero-elastic model is discussed in this study. A detailed description of the instrumentations, boundary conditions, and the data acquisition system used in the test is provided. The profiles of the downburst radial velocities measured at different distances is provided and the location of the peak radial wind speed is determined. A review about the built in-house numerical models, that were previously developed to evaluate the response of transmission towers and their attached conductors when subjected to a generic downburst, is provided. The main findings of the numerical studies conducted using those numerical models is discussed. In order to validate these findings, three test layouts are selected to assess the response of the transmission line to different downburst configurations representing varying distances measured between the centers of the downburst and the study tower. The study configurations also consider eleven downburst angles of attack. The following summarizes the findings of this study:

- The time history response of tower shows a typical trend where a sudden peak occurs then the response reaches a sudden minimum peak.
- The downburst wind speeds as well as the corresponding response of the tower are decomposed into running-mean and fluctuating components by adopting a cutting-off frequency greater than the shedding frequency of the main vortices of the downburst.
- The experiment results show that the main shaft of the tower experiences a critical response under an angle of attack of  $90^\circ$ .
- For the angle of attack of  $0^\circ$  where one tower leg is shielded behind the other, the shielding factor is found to be in order of 0.7~0.8. A more dedicated study is needed to accurately assess

this aspect for the lattice transmission towers.

- The oblique angle of attack induces a significant longitudinal force in the conductors that causes an out-of-plan moment at the cross arm sections. This longitudinal force is found to be as high as 58% of the conductor's transverse force.
- The results show that the critical responses of the tower sections may occur under different cases of loadings. This might be of importance for the design guidelines committees responsible for determining the loading importance factors.
- The structural system of the tower of this study minimizes the vulnerability of the tower to the downburst. This is because the majority of the conductor's and the cross arm forces transfer directly to the guys supports and consequently to the foundations.
- Four test cases are used to validate the built in-house numerical models. The mean component of the downburst wind field measured at the WindEEE dome is implemented into the in-house numerical models to provide similar wind pressure to that occurred during the test. The validation shows a very good agreement between the measured responses of the tower and the calculated responses using the numerical models.
- Similar validation process is conducted for the peak responses. The peak wind velocities are implemented in the numerical models to simulate the wind pressures applied on the tested model. The validation shows a good agreement between both the test results and the calculated responses using the numerical model. The error is believed to be due to the quasi-static assumption taken in the numerical model solution.
- The discrepancies between the measured and the calculated responses increase in the oblique load cases where a significant conductor forces contributes to the tower response. This is may be attributed to the accuracy in estimating the wind forces used in the numerical models.

## Acknowledgments

The authors would like to thank the generous financial support received from the company Hydro One and the Natural Science and Engineering Research Council of Canada (NSERC) to complete this project. The authors also are very grateful for experts at the Boundary Layer Wind Tunnel lab (BLWTL) and the Wind Engineering, Energy and Environment Research Institute (WindEEERI) for their guidance throughout the stages of this project.

## References

Abd-Elaal, E., Mills, J.E. and Ma, X. (2013), "An analytical model

- for simulating steady state flows of downburst", *J Wind Eng Ind Aerod.*, **115**, 53-64.
- Aboshosha, H. and El Damatty, A.A. (2014), "Effective numerical technique to analyse transmission line conductors under high intensity winds", *Wind Struct.*, **18**(3), 235-252.
- Aboshosha, H. and El Damatty, A.A. (2015a), "Dynamic response of transmission line conductors under downburst and synoptic winds", *Wind Struct.*, **21**(2), 241-272.
- Aboshosha, H. and El Damatty, A. (2015b), "Engineering method for estimating the reactions of transmission line conductors under downburst winds", *Eng. Struct.*, **99**, 272-284.
- Aboshosha, H., Bitsuamlak, G. and El Damatty, A. (2015a), "Turbulence characterization of downbursts using LES", *J. Wind Eng. Ind. Aerod.*, **136**, 44-61.
- American Society of Civil Engineers (ASCE) (2010), "Guidelines for electrical transmission line structural loading", ASCE manuals and reports on engineering practice, No. 74, New York, NY, USA.
- Australian Wind Alliance (2016), <http://www.windalliance.org.au/>
- Chay, M., Albermani, F. and Wilson, R. (2006), "Numerical and analytical simulation of downburst wind loads", *Eng. Struct.*, **28**(2), 240-254.
- Chay, M. and Letchford, C. (2002), "Pressure distributions on a cube in a simulated thunderstorm downburst - part a: stationary downburst observations", *J. Wind Eng. Ind. Aerod.*, **90**, 711-732.
- Choi, E. and Hidayat, F. (2002), "Dynamic response of structures to thunderstorm winds", *Prog. Struct. Eng. Mech.*, **4**, 408-416.
- Darwish, M. and El Damatty, A. (2011), "Behavior of self-supported transmission line towers under stationary downburst loading", *Wind Struct.*, **14**(5), 481-484.
- Didden, N. and Ho, C.M. (1985), "Unsteady separation in a boundary layer produced by an impinging jet", *J. Fluid Mech.*, **160**, 235-256.
- Donaldson, C. and Snedeker, R. (1971), "A study of free jet impingement, Part 1. Mean properties of free and impinging jets", *J. Fluid Mech.*, **45**, 281-319.
- Elawady, A., Aboshosha, H., El Damatty, A., Bitsuamlak, G., Hangan, H. and Elatar, A. (2017), "Aeroelastic testing of Multi-spanned transmission line subjected to downbursts", *J. Wind Eng. Ind. Aerod.*, **169**, 194-216. doi.org/10.1016/j.jweia.2017.07.010
- Failure Investigation Report, HYDRO ONE NETWORKS INC (2006), "Failure of towers 610 and 611, circuit X503E – 500 kV guyed towers near the Township of Waubashene", Ontario, August 2, 2006", Line Engineering.
- Fujita, T. (1985), "The downburst: microburst and macroburst", SMRP Research Paper 210, University of Chicago, USA.
- Fujita, T. (1990), "Downbursts: meteorological features and wind field characteristics", *J. Wind Eng. Ind. Aerod.*, **36**, 75-86.
- Gant, S. (2009), "Reliability issues of LES-related approaches in an industrial context", *Flow. Turbul. Combust.*, **84**, 325-335.
- Gerges, R. and El-Damatty, A. (2002), "Large displacement analysis of curved beams", *Proceedings of the Canadian Society of Civil Engineering Conference, Montreal, Canada*, ST 100.
- Hangan, H., Roberts, D., Xu, Z. and Kim, J. (2003), "Downburst simulation. Experimental and numerical challenges", *Proceedings of the 11th International Conference on Wind Engineering*, Lubbock, TX, USA.
- Hjelmfelt, M. (1988), "Structure and life cycle of microburst outflows observed in Colorado", *J. Appl. Meteorol.*, **27**, 900-927.
- Holmes, J. (2008), "Recent developments in the specification of wind loads on transmission lines", *J. Wind Eng. Ind. Aerod.*, **8**-18.
- Holmes, J., Hangan, H., Schroeder, J., Letchford, C. and Orwig, K. (2008), "A forensic study of the Lubbock-Reese downdraft of 2002", *Wind Struct.*, **11**(2), 137-152.
- Ivan, M. (1986), "A ring-vortex downburst model for flight simulations", *J. Aircraft*, **23**, 232-236.
- Kanak, J., Benko, M., Simon, A. and Sokol, A. (2007), "Case study of the 9 May 2003 windstorm in southwestern Slovakia", *Atmos. Res.*, **83**, 162-175.
- Kim, J. and Hangan, H. (2007), "Numerical simulations of impinging jets with application to downbursts", *J. Wind Eng. Ind. Aerod.*, **95**(4), 279-298.
- Koziey, B. and Mirza, F. (1994), "Consistent curved beam element", *Comput. Struct.*, **51**(6), 643-654.
- Kwon, D. and Kareem, A. (2009), "Gust-front factor: new framework for wind load effects on structures", *J. Struct. Eng. – ASCE*, **135**(6), 717-732.
- Mara, T. and Hong H. (2013), "Effect of wind direction on the response and capacity surface of a transmission tower", *Eng. Struct.*, **57**, 493-501.
- Mason, M., Wood, G. and Fletcher, D. (2010), "Numerical investigation of the influence of topography on simulated downburst wind fields", *J. Wind Eng. Ind. Aerod.*, **98**(1), 21-33.
- Mason, M., Wood, G. and Fletcher, D. (2009), "Numerical simulation of downburst winds", *J. Wind Eng. Ind. Aerod.*, **97**(11-12), 523-539.
- McCarthy, P. and Melsness, M. (1996), "Severe weather elements associated with September 5, 1996 hydro tower failures near Grosse".
- Oseguera, R. and Bowles, R. (1988), "A simple, analytics 3-dimensional downburst model based on boundary layer stagnation flow" NASATM- 100632. Hampton (VA): NASA Langley Research Center.
- Savory, E., Parke, G., Zeinoddini, M., Toy, N. and Disney, P. (2001), "Modelling of tornado and microburst-induced wind loading and failure of a lattice transmission tower", *Eng. Struct.*, **23**(4), 365-375.
- Sengupta, A. and Sarkar, P. (2008), "Experimental measurement and numerical simulation of an impinging jet with application to thunderstorm microburst winds", *J. Wind Eng. Ind. Aerod.*, **96**, 345-365.
- Shehata, A. and El Damatty, A. (2008), "Failure analysis of a transmission tower during a microburst", *Wind Struct.*, **11**(3), 193-208.
- Shehata, A.Y. and El Damatty, A.A. (2007), "Behaviour of guyed transmission line structures under downburst wind loading", *Wind Struct.*, **10**(3), 249-268.
- Shehata, A.Y., El Damatty, A.A. and Savory, E. (2005), "Finite element modeling of transmission line under downburst wind loading", *Finite Elem. Anal. Des.*, **42**(1), 71-89.
- Solari, G., Burlando, M., De Gaetano, P. and Repetto, M.P. (2015), "Characteristics of thunderstorms relevant to the wind loading of structures", *Wind Struct.*, **20**(6), 763-791.
- Vermeire, B., Orf, L. and Savory, E. (2011a), "Improved modelling of downburst outflows for wind engineering applications using a cooling source approach", *J. Wind Eng. Ind. Aerod.*, **99**, 801-814.
- Wang, X., Lou, W., Li, H. and Chen, Y. (2009), "Wind-induced dynamic response of high-rise transmission tower under downburst wind load", *J. Zhejiang Univ.*, **43**(8), 1520-1525.
- Wood, G., Kwok, K., Motteram, N. and Fletcher, D. (2001), "Physical and numerical modelling of thunderstorm downbursts", *J. Wind Eng. Ind. Aerod.*, **89**, 535-552.
- Yang, F.G. and Zhang, H.G. (2016), "Two case studies on structural analysis of transmission towers under downburst", **22**(6), 685-701.
- Zhang, Y. (2006), "Status quo of wind hazard prevention for transmission lines and counter measures", *East China Electric Power*, **34**(3), 28-31.